Physics AUC, vol. 17 (part I), 44-58 (2007) PHYSICS AUC

Interpretation of heat losses from open chaotic systems

A. Wingen[1], K.H. Spatschek[1], S.S. Abdullaev[2] and M. Jakubowski[2]

[1]Institut für Theoretische Physik, Heinrich-Heine-Universität Düsseldorf, D–40225 Düsseldorf, Germany

[2]Institut für Plasmaphysik, Forschungszentrum, Jülich GmbH, EURATOM Association, Trilateral Euregio Cluster, D–52425, Jülich, Germany

Abstract

Heat fluxes on divertor plates of tokamaks show typical structures being related to the topology of large connection lengths of magnetic field lines. The selection of those areas of large connection lengths which ultimately determine the heat flux pattern is due to the unstable and stable manifolds of the hyperbolic fixed points of the last intact island chain. The manifolds attract co- (with respect to the magnetic field direction) and counter-moving particles, respectively. Analyzing the footprints of the manifolds, one can predict areas of large heat depositions in agreement with experiments.

1 Introduction

The interpretation of observed particle and heat transport phenomena is a central problem in many branches of physics. Very often the transport is anomalous [1], i.e. it does not agree with results from linear response theory [2]. As is well-known from dynamics of nonlinear systems, characteristic patterns may be formed [3]-[4]. Spatial, temporal, or spatio-temporal structures can occur. Several selection rules and normal forms for pattern formation have been formulated in different disciplines, e.g. optics, plasmas, fluids, soft matter, and so on. They establish the first step from a purely descriptive to a predictive nonlinear transport theory.

Nonlinear signatures of particle and heat transport are almost generic in plasma and astrophysics. Transport anomalies reach from Bohm-like diffusion in gas discharges up to low-energy cosmic ray penetration into the heliosphere [5]-[6]. Because of the available advanced diagnostic techniques, especially in existing tokamaks, a lot of experimental material on nonlinear transport is available from laboratory plasma science; see e.g. Ref. [7] and references therein. For magnetic fusion, heat flux investigations are important since the wall load should be within a tolerable regime. The use of edge stochastization may be a possible solution to the plasma-wall-interaction control [8]. By stochastization of the plasma edge the heat and particle flows to the wall are fundamentally changed [9], [1],

[10]. Still many problems are open, and therefore the basic physical principles of transport in open chaotic systems need further consideration.

Magnetic field lines represent a $1 + \frac{1}{2}$ -degrees–of–freedom Hamiltonian system [3]. This fact is important for the description of field lines by flux–preserving mappings which are computationally efficient and powerful tools to study field lines in the presence of non–axisymmetric magnetic perturbations. Several mapping models of field lines in a toroidal system have been proposed to study the destruction of nested magnetic surfaces and the formation of stochastic magnetic field lines (see Refs. [11]-[18] and references therein). A discrete iterative map runs much faster then the small-step numerical integration [13], [16], [19], [20]. Mappings should be symplectic (or flux-preserving). They should have the same periodic points as the Poincaré map of the original system, and they should show the same regular and chaotic regions as the continuous magnetic field line evaluation. For global maps, a magnetic axis should be mapped to itself, and the magnetic flux should be always positive [11].

An important aspect of transport is the dynamics of particles in a stochastic magnetic field. It is known that in inhomogeneous magnetic fields particle orbits deviate from the magnetic field lines [21]. An interesting question is how this can affect the transport of particles in a stochastic magnetic field. The enhanced transport of heat and particles due to destroyed nested magnetic surfaces has been analyzed in the past in a number of publications (see Refs. [22]-[29]). In a weakly collisional plasma, charged particles gyrate around the magnetic field lines. Since the gyro-radius scales with the magnetic field strength, for magnetic fields of the order of tesla the gyro-radii (especially for electrons) are very small compared to the dimensions of the system. Because of the curvature and gradients of the magnetic field, the particles are drifting away from the magnetic surfaces. In the gyro-center approximation, one neglects finite gyro-radius effects. For integrable situations, the deviations of the drift surfaces from the magnetic KAM surfaces increase with the particle energy. The kinetic energy of the particles is therefore, in addition to the perturbation current for the stochastic magnetic field generation, an important parameter for the break-up of drift surfaces. In a fusion plasma of typically $kT = 10 - 20$ keV temperature, most of the particles move with the thermal velocity. According to recent studies of particle drift effects [30]-[31] only particles with kinetic energies much larger than the thermal one show relevant drift effects. Thus, thermal particles follow very well the field line dynamics.

Characteristic spatial heat flux patterns have been observed in bounded stochastic plasmas [32]-[33]. They show a characteristic number of stripes on the target plates when plotted in the (φ, θ)-plane, where φ is the toroidal angle and θ is the poloidal angle of the torus. In addition, when varying the edge safety factor q_a, and projecting on the (q_a, θ)-plane, generic structures appear. In order to analyze and classify the spatial structures of heat flux patterns [33], we will use the concept of magnetic footprints [34], [35] together with an analysis of the stable and unstable manifolds of hyperbolic periodic points [36]-[39] of magnetic resonances present in the stochastic plasma edge region.

The paper is organized as follows. We shortly describe the phenomenology of heat flux patterns at the divertor plates of TEXTOR-DED and the magnetic field configuration in Sec. 2. In Sec. 3 we outline the mapping technique and the numerical methods for calculating stable and unstable manifolds. The relation of large connection lengthes to the measured heat flux patterns and the selection criterion provided by the stable and unstable manifolds is discussed in Sec. 4. The structures of the pattern are analyzed by

the stable and unstable manifolds of the resonances in the ergodic chaotic edge region. Especially the manifolds of the last island chain in the ergodic zone, being located at the transition to the laminar zone, are important. The paper is concluded by a short summary.

2 Magnetic field lines and heat flux patterns

It is known that a divergence–free magnetic field is equivalent to a Hamiltonian system with 1+1/2 degrees of freedom (see, e.g., [40], [41], [42]). Particularly, the magnetic field $\mathbf{B}$ has can be presented in the Clebsch form $\mathbf{B} = B_0 R_0^2 \left(\nabla\psi \times \nabla\vartheta + \nabla\varphi \times \nabla\psi_{pol}\right)$, where ψ and ψ_{pol} are the normalized to $B_0 R_0^2$ toroidal and poloidal fluxes, respectively, ϑ is the poloidal (intrinsic) angle angle θ, and φ is the toroidal angle. Here B_0 is the strength of the toroidal magnetic field at the center of torus R_0. In this coordinate system the field line equations have the Hamiltonian form

$$\frac{d\psi}{d\varphi} = -\frac{\partial H}{\partial \vartheta} \qquad \frac{d\vartheta}{d\varphi} = \frac{\partial H}{\partial \psi}, \tag{1}$$

where the poloidal flux $H \equiv \psi_{pol}$ plays the role of an Hamiltonian function, ϑ and ψ are canonically conjugated coordinate and momentum, respectively, and φ is a time-like independent variable.

In the presence non-axisymmetric magnetic perturbations the poloidal flux $H = H(\psi, \vartheta, \varphi)$ can be presented as sum

$$H = H_0(\psi) + H_1(\psi, \vartheta, \varphi), \tag{2}$$

where the unperturbed flux $\psi_{pol}^{(0)}(\psi)$ depends only on the equilibrium magnetic configuration of the plasma. It is determined by the safety factor $q(\psi)$:

$$H_0(\psi) = \int \frac{d\psi}{q(\psi)}. \tag{3}$$

The perturbation flux $\psi_{pol}^{(1)}(\psi, \vartheta, \varphi)$ can be expanded into a Fourier series in ϑ and φ:

$$H_1(\psi, \vartheta, \varphi) = \epsilon \sum_{m,n} H_{mn}(\psi) \cos(m\vartheta - n\varphi + \chi_{mn}). \tag{4}$$

The Fourier coefficients $H_{mn}(\psi)$ correspond to the poloidal mode number m and the toroidal mode number n.

2.1 The equilibrium plasma configuration and magnetic perturbations

We model the plasma with nested, circular magnetic surfaces with the outward (Shafranov) shift of magnetic surfaces due to effects of the plasma pressure and electric current. Let a and $R_0(a)$ be the plasma minor radius and the major radius of the center of the last magnetic surface, respectively. Then, the shift $\Delta(\rho)$ of the major radius of the center of the magnetic surface of radius ρ form $R_0(a)$ is given by [43]

$$\Delta(\rho) = \left[R_0^2(a) + (\Lambda + 1)\left(a^2 - \rho^2\right)\right]^{1/2} - R_0(a), \tag{5}$$

where $\Lambda = \beta_{pol} + l_i/2 - 1$, $\beta_{pol} = 8\pi\langle p\rangle/\langle B_\theta\rangle^2$ is the ratio of the plasma pressure $\langle p\rangle$ to the magnetic pressure $\langle B_\theta\rangle^2/8\pi$ of the poloidal field B_θ, l_i is the internal inductance. Furthermore, we consider only the low–β and large aspect-ratio tokamak plasma.

In the cylindrical coordinate system (R, φ, Z) the magnetic field of the equilibrium plasma can be presented by the vector potential,

$$\begin{aligned} \mathbf{A} &= (0, A_\varphi(r,\theta), A_z(r,\theta))\,, \\ A_\varphi(r,\theta) &= \frac{B_0 R_0^2}{R}\int \frac{d\psi}{q\,(\rho(\psi))}, \\ A_z(r,\theta) &= -B_0 R_0 \ln(R/R_0). \end{aligned} \tag{6}$$

where r, θ are toroidal coordinates related to (R, Z): $R = R_0 + r\cos\theta, Z = r\sin\theta$, $A_z(r,\theta)$ corresponds to the toroidal field $B_\varphi = B_0 R_0/R$, and $A_\varphi(r\theta)$ corresponds to the poloidal field,

$$B_\theta(r,\theta) = \frac{B_0}{qR}\frac{d\psi}{d\rho}\frac{1}{1+\Delta'(\rho)\cos\bar{\theta}}, \tag{7}$$

where $\bar{\theta} = \sin^{-1}(r\sin\theta/\rho)$. One should note that the Hamiltonian function of field lines is expressed through the toroidal component of the vector potential via $H = -RA_\varphi/B_0R_0^2$.

The safety factor $q(\rho)$ is a function of the radius ρ of a magnetic surface which is related to the normalized toroidal magnetic flux ψ:

$$\psi = \frac{R_0(\rho)}{R_0(a)}\left[1 - \left(1 - \frac{\rho^2}{R_0^2(\rho)}\right)^{1/2}\right] \approx \frac{\rho^2}{2R_0^2(a)}. \tag{8}$$

The relation between ρ and the toroidal coordinates (r,θ) is
$\rho = \sqrt{(r\cos\theta - \Delta(\rho))^2 + r^2\sin^2\theta}$.

In a cylindrical plasma one can use the following model for the safety factor (see [21])

$$\begin{aligned} q_{cyl}(\rho) &= q_a\frac{\rho^2}{a^2}\left[1 - \left(1 - \frac{\rho^2}{a^2}\right)^{\nu}\right]^{-1}, \text{ for } \rho \le a\,, \\ q_{cyl}(\rho) &= q_a\frac{\rho^2}{a^2}, \text{ for } \rho > a\,. \\ q_a &= \frac{2\pi B_0 R_0 a^2}{\mu_0 I_p}, \end{aligned} \tag{9}$$

where q_a is the safety factor at the plasma edge a, I_p is the total plasma current, and the exponent is $\nu = q_a/q_0$.

The safety factor given by Eq. (9) is valid only for the cylindrical plasma column. For large aspect–ratios $R/r \gg 1$ the safety factor due to toroidicity can be presented as a series of powers of the inverse aspect ratio $\varepsilon = \rho/R_p(\rho)$ (see Ref. [44]) :

$$q(\rho) = q_{cyl}(\rho)\frac{R_0^2}{R_p^2(\rho)}\left(1 + \frac{a_2}{2}\varepsilon^2 + \frac{3a_4}{8}\varepsilon^4 + O(\varepsilon^8)\right), \tag{10}$$

where $q_{cyl}(\rho)$ is described by (9) and the coefficients a_m are given by

$$a_m = (-1)^m\sum_{k=0}^{m}(m-k+1)\Lambda^k. \tag{11}$$

According to Refs. [44], [17], the static perturbation magnetic field created by the external TEXTOR-DED coils without the plasma response is mainly determined by its toroidal component of the vector potential $A_\varphi^{(pert)}(r,\theta,\varphi)$. The normalized to $B_0R_0^2/R$ vector potential, i.e. $f_\varphi^{(1)} = B_0R_0^2A_\varphi^{(pert)}/R$, is approximated as

$$f_\varphi^{(1)}(r,\theta,\varphi) = \varepsilon\sum_m f_m(r,\theta)\cos(m\theta - n\varphi + \chi_{mn}) \tag{12}$$

with the Fourier modes

$$f_m(r,\theta) = -\frac{r_c}{mR_0}g_m\sqrt{1+\frac{r_c\cos\theta}{R_0}}\left(\frac{r}{r_c}\right)^m \ , \tag{13}$$

$$g_m = (-1)^m\frac{\sin\left[(m-nm_0/4)\theta_c\right]}{(m-nm_0/4)\pi} \ . \tag{14}$$

Here $\varepsilon = B_c/B_0$ stands for the perturbation parameter, $B_c = \mu_0 I_d m_0/(\pi r_c)$ is the characteristic value of the DED magnetic field perturbation, r_c is the minor radius of the DED-coils, $\theta_c \approx \pi/5$ is the half angle area of the coils, $m_0 \approx 20$, I_d is the DED current.

The Fourier coefficients $H_{mn}(\psi)$ of the perturbation Hamiltonian (4) are related to the coefficients $f_m(r,\theta)$ through the Fourier integrals

$$H_{mn}(\psi) = \frac{1}{2\pi}\sum_{m'}\int_0^{2\pi} f_{m'}(r,\theta)e^{i(m'\theta(\vartheta)-m\vartheta}d\vartheta. \tag{15}$$

where the geometrical toroidal angle $\theta(\vartheta)$ is a function of the intrinsic poloidal angle ϑ which depends on the equilibrium plasma.

The properties of the mode transformation of the spectra of perturbations $f_{m'}(r,\theta)$ in the geometrical space to the $H_{mn}(\psi)$ in intrinsic coordinates have been studied in Refs. [44], [17], [45].

2.2 Heat flux patterns

There are three operational regimes of the TEXTOR-DED which are called 12/4, 6/2, and 3/1 modes corresponding to the regimes with the dominant toroidal mode numbers $n = 4, n = 2, n = 1$, respectively (see Refs. [46], [47], [17]). Below we will mainly consider the 12/4 mode of the DED for the dominant toroidal mode number $n = 4$. In this regime four heat flux stripes are observed at the divertor plates [48]. Concentrating on one of these stripes, the development of the heat flux at a fixed toroidal position with changing plasma current has been measured [49]. The pattern is taken at a fixed toroidal position over the small poloidal angle area covered by one heat flux stripe. The edge safety factor q_a is inversely proportional to the plasma current (see Eq. (9)), which is varied during the measurements. All other parameters are kept constant at typical values: toroidal magnetic field $B_0 = 1.93$ T, minor radius of plasma $a = 0.437$ m, major radius of plasma $R_a = 1.7$ m and $\Lambda = 0.05$. The divertor plates (in the following also called wall) are located at a minor radius of $r_w = 0.477$ m.

In typical measurements [49] we see that at certain values of q_a new strike zones appear, while the former strike zones tend outwards (compared to the center of the pattern), get smaller, and finally vanish. The strike zones are overlapping, which means that the next strike zone appears, while the last one has not yet vanished. These structures of the heat flux pattern can be explained by the theory of the stable and unstable manifolds.

3 Stable and unstable manifolds

In this section we study the stochasticity of field lines created by the external magnetic perturbations at the plasma edge. This will be done by plotting Poincaré sections of magnetic field lines and their stable and unstable manifolds. For this purpose we shall employ the computationally efficient mapping method described in Refs. [50], [51], [45]. The mapping is constructed in a symplectic (or flux-preserving) form and it is much faster than the other conventional small-step integration schemes, like Runge-Kutta. Below, we shall shortly outline the mapping method. We will use it for finding periodic fixed points and their stable and unstable manifolds.

3.1 Discrete mapping

Let (ϑ_k, ψ_k) be values of the poloidal angle ϑ and the toroidal flux ψ at the poloidal section $\varphi = \varphi_k = k(2\pi/N)$, where $k = 0, \pm 1, \pm 2, \ldots$, and $N \geq 1$. The relation

$$(\vartheta_{k\pm1}, \psi_{k\pm1}) = \hat{T}^{(\pm)}(\vartheta_k, \psi_k), \tag{16}$$

defines the mapping of the field line coordinates at the section φ_k to the ones at the section $\varphi_{k\pm1}$. The sign $(+)$ corresponds to the mapping along the positive direction of the toroidal angle φ, and it is called as a *forward map*. Similarly, the sign$(-)$ corresponds a *backward map* which describes field line dynamics along the negative direction of the toroidal angle.

The mapping (16) is implemented by the successive canonical transformations employing the time-dependent perturbation theory. For the Hamiltonian system (2)-(4) the mapping, in the first order of the perturbation parameter ϵ, has the following form

$$\begin{aligned} \Psi_k = \psi_k - \epsilon\frac{\partial S^{(k)}}{\partial \vartheta_k}, \Theta_k = \vartheta_k + \epsilon\frac{\partial S^{(k)}}{\partial \Psi_k}, \bar{\Theta}_k = \Theta_k + \frac{\varphi_{k\pm1} - \varphi_k}{q(\Psi_k)}, \\ \psi_{k\pm1} = \Psi_k + \epsilon\frac{\partial S^{(k\pm1)}}{\partial \vartheta_{k+1}}, \vartheta_{k\pm1} = \bar{\Theta}_k - \epsilon\frac{\partial S^{(k\pm1)}}{\partial \Psi_{k\pm1}}, \end{aligned} \tag{17}$$

where $S^{(k)} \equiv S(\vartheta_k, \Psi_k)$ is the value of the generating function $S(\vartheta, \Psi, \varphi, \varphi_0)$ taken at sections $\varphi = \varphi_k$, i.e. $S(\vartheta_k, \Psi_k) = S(\vartheta_k, \Psi_k, \varphi_k, \varphi_0)$,

$$\begin{aligned} S(\vartheta, \Psi, \varphi, \varphi_0) = -(\varphi - \varphi_0) \sum_{m,n} H_{mn}(\Psi) \times \Big[a(x_{mn}) \sin\left(m\vartheta - n\varphi + \chi_{mn}\right) \\ + b(x_{mn}) \cos\left(m\vartheta - n\varphi + \chi_{mn}\right) \Big], \end{aligned} \tag{18}$$

defined in the finite interval $\varphi_{k+1} < \varphi < \varphi_k$. Here

$$\begin{aligned} a(x) = \frac{1 - \cos x}{x}, \qquad b(x) = \frac{\sin x}{x}, \\ x_{mn} = \left(\frac{m}{q(\Psi)} - n\right)(\varphi - \varphi_0). \end{aligned}$$

The free parameter φ_0 lies in the interval $\varphi_k \leq \varphi_0 \leq \varphi_{k+1}$.

The Poincaré section corresponding to the pre-selected poloidal section φ_P is obtained by applying the map (16) N times, when field lines return the poloidal section φ_P.

3.2 Fixed Points and their stable and unstable manifolds

A periodic fixed point with period n is defined through

$$\psi = M_\psi^n(\psi, \vartheta)\,, \qquad \vartheta = M_\vartheta^n(\psi, \vartheta) \mod 2\pi\,, \tag{19}$$

with M_ψ^n and M_ϑ^n being the n-times iterations of the map with respect to ψ and ϑ, respectively. There are two different kinds of fixed points. The elliptic ones, which are at the centers of the islands, are stable. A field line very close to the elliptic point will iterate on an elliptic orbit around that fixed point and will always stay close to it. At the moment, elliptic fixed points are of no further interest to us. The hyperbolic ones, i.e. the intersection points of the unperturbed separatrix, are located between the islands. They are unstable. A field line close to the hyperbolic point will follow a hyperbolic orbit away from the fixed point. These points and their unstable manifolds are the source of chaos and anomalous transport [37].

Finding the hyperbolic points is extremely difficult due to their unstable character. But they can be determined numerically using a minimization method [52], [53]. The problem is similar to solving a system of N nonlinear equations ($N = 2$ here)

$$F_i(\vec{x}) = F_i(x_1, x_2, \ldots, x_N) = 0 \quad 1 \le i \le N\,. \tag{20}$$

We have to minimize

$$f(\vec{x}) = \sum_{i=1}^{N} (F_i(\vec{x}))^2\,. \tag{21}$$

Therefore we consider the function

$$g(t) = f(\vec{a} + t \cdot \vec{d})\,, \tag{22}$$

where $\vec{a} = (a_1, \ldots, a_N)$ is a chosen starting point and $\vec{d} = (d_1, \ldots, d_N)$ is a chosen directional vector. Now we have to find the minimum t_{min} of $g(t)$. The next starting point is then given by $\vec{a}_1 = \vec{a} + t_{min} \cdot \vec{d}$, and we have to choose a new direction $\vec{d}_1$ in which the one-dimensional minimization is then performed. To ensure the convergence, the proper choice of the direction is important. The native choice for the direction would be the gradient

$$\vec{d} = -\nabla f(\vec{a})\,, \tag{23}$$

but the conjugated direction method [52], which is outlined in the following, is more effective.

For one N-dimensional minimization step, we use N sub-steps

- Sub-step 0:

  For the starting point $\vec{x}_0$, we choose the direction

  $$\vec{d}_0 = -\nabla f(\vec{x}_0).$$

By minimizing the function

$$g_0(t) = f(\vec{x}_0 + t \cdot \vec{d}_0)$$

with respect to t, we get the new starting point

$$\vec{x}_1 = \vec{x}_0 + t_{min} \cdot \vec{d}_0.$$

- Sub-step $k+1$ ($k < N-1$):

  Using the directional vector

  $$\vec{d}_{k+1} = -\nabla f(\vec{x}_{k+1}) + \beta_k \vec{d}_k$$

  with

  $$\beta_k = \frac{||\nabla f(\vec{x}_{k+1})||^2}{||\nabla f(\vec{x}_k)||^2}$$

  we minimize $g_{k+1}(t) = f(\vec{x}_{k+1} + t \cdot \vec{d}_{k+1})$ with respect to t and calculate $\vec{x}_{k+2} = \vec{x}_{k+1} + t_{min} \cdot \vec{d}_{k+1}$.

These steps are performed up to $N-1$, then the procedure starts again at sub-step 0 with $\vec{x}_0 = \vec{x}_N$.

The one-dimensional minimization is performed in each sub-step using Newton's method to find the vanishing of the first derivative $g'(t)$. Normally the second derivative $g''(t)$ is needed for Newton's method. With $\vec{y} = \vec{x} + t \cdot \vec{d}$ we obtain

$$g'(t) = \nabla f(\vec{y}) \cdot \vec{d} = 2 \sum_{i,j=1}^{N} \frac{\partial F_j}{\partial x_i}(\vec{y}) F_j(\vec{y}) d_i \tag{24}$$

and

$$g''(t) = 2 \sum_{i,j,l=1}^{N} \frac{\partial^2 F_j}{\partial x_i \partial x_l}(\vec{y}) F_j(\vec{y}) d_i d_l + 2 \sum_{i,j,l=1}^{N} \frac{\partial F_j}{\partial x_i} \frac{\partial F_j}{\partial x_l}(\vec{y}) d_i d_l \; . \tag{25}$$

One can neglect the first term on the right-hand-side of the second derivative, so that the second derivative can be approximated by products of the first derivatives. Note that all values are those of the actual sub-step.

Using this simplification we can approximate t_{min} by

$$t_{min} = -\frac{g'(0)}{\tilde{g}''(0)} \; , \tag{26}$$

with

$$\tilde{g}''(t) = 2 \sum_{i,j,l=1}^{N} \frac{\partial F_j}{\partial x_i} \frac{\partial F_j}{\partial x_l}(\vec{y}) d_i d_l \; . \tag{27}$$

This procedure converges very fast and will lead to both types of fixed points up to the desired accuracy. The fixed point being found depends on the choice of the first starting point. The best way to find fixed points in a certain area is to use a grid of starting points.

Figure 1 shows a typical Poincaré plot for the magnetic field lines of the stochastic plasma edge in TEXTOR. Three main resonances can be observed: the 10/4 island chain, which is the last resonance in front of the wall, already in the laminar zone, the 9/4 island chain at the transition to the laminar zone, and the 8/4 resonance close to the last closed flux surface. The elliptic and hyperbolic points of the period 9 island chain are marked.

The hyperbolic points are the source of chaos. Around them the chaos appears. Due to the slightest perturbation, the separatrix splits into the stable and unstable manifolds. The unstable manifold of a hyperbolic periodic fixed point is defined as the set of points

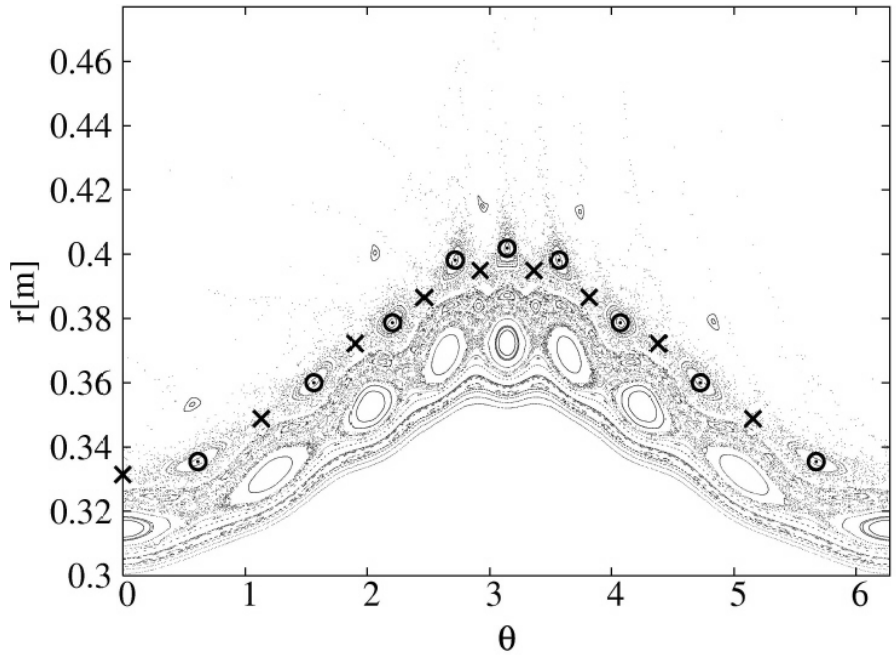

Figure 1: Poincaré section of the TEXTOR-DED magnetic field at $q_a = 3.03$. The period 9 elliptic points (circles) and hyperbolic points (crosses) are marked.

which converge under the map towards the fixed point for $n \to -\infty$. The stable manifold is the unstable manifold of the inverse map.

The manifolds show an oscillatory behavior close to a hyperbolic point [37]. The oscillations of the stable and unstable manifold intersect infinite times, while the area enclosed by the intersection is preserved. Field lines within such enclosed areas are iterating from one area to another [38]. Because the areas are getting very long and extremely thin, close to the fixed point (note the increasing amplitude of the oscillations and the area preserving property) two neighboring field lines are located in different areas and therefore iterate in completely different ways.

Examples of a stable and an unstable manifold can be see in Fig. 2. The manifolds oscillate around the period 9 islands, pass the last island chain with large loops and hit the wall of the tokamak which is located at the top of the figure.

To calculate the unstable manifold of a hyperbolic fixed point with period n, we choose a starting-point $\vec{x}$ very close to the hyperbolic fixed point and calculate the $2n$-th iterate $\vec{y}$ of $\vec{x}$. Therefore we must know the position of the hyperbolic point precisely. The line-element between $\vec{x}$ and $\vec{y}$ then approximates the unstable manifold very well, and by iterating the line-element we get the unstable manifold [36], [37].

4 Manifold-wall-interaction

According to [37], the stable and unstable manifolds have infinite connection lengthes, and field lines close by have very large ones too. Strike points of the stable and unstable manifolds with the wall should lie in the areas of large connection lengths. Further, the field lines are following the unstable manifolds to the wall [37]. Since the manifolds deeply

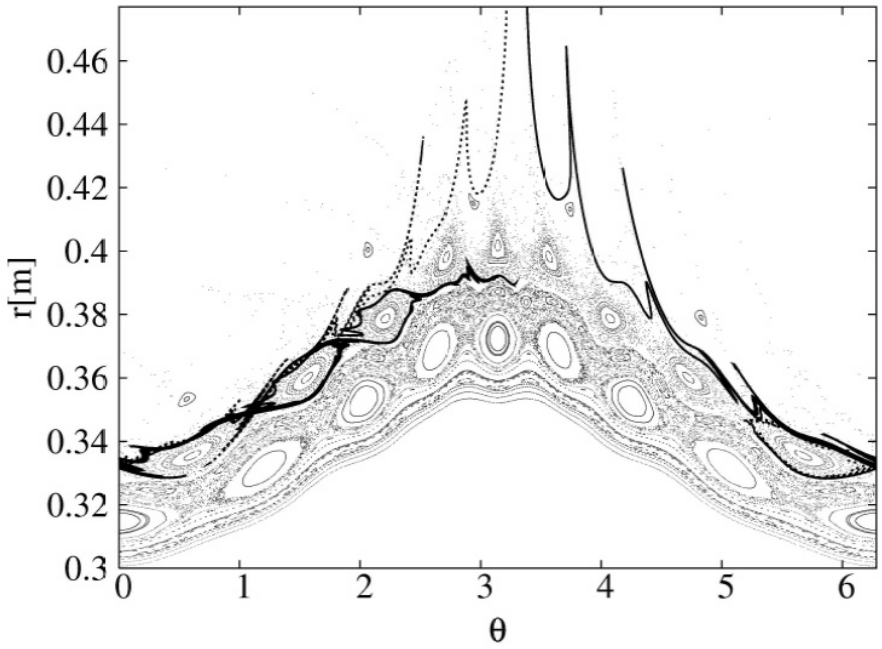

Figure 2: Same Poincaré section as Fig. 1, now with a stable (dashed line) and an unstable manifold (solid line) of the period 9 island chain.

penetrate into the plasma, a large amount of heat deposition will be at the strike points of the manifolds. But not only the unstable manifolds are important. The plasma particles are either co-passing or counter-passing [30], [31], which means that they are either moving in the direction of the field lines (following the unstable manifold), or against (following the stable manifold). Note that the stable manifold is the unstable one for the reverse direction [37]. So, we conclude that large connection lengthes are necessary for significant heat loads in order to have an efficient transport from the (inner) hot plasma to the (outer) cold boundary. But large connection lengths are not sufficient as we will see when discussing the inner branches

For the interpretation the following observation is of great interest. In the Poincaré section of Fig. 2 we showed (besides some field line intersections) continuous manifolds, however only up to the first wall contact. A specific magnetic field line escaping from the plasma will pierce the plane at discrete points close to the unstable manifold of a hyperbolic fixed point of the last resonant island chain. When continuing, e.g. the unstable manifold, beyond the first wall contact, an additional part of the manifold appears which turns around in a loop and re-enters the system (until it leaves the system again). An additional intersection of the manifold with the wall occurs. This is shown in Fig. 3 for an unstable manifold of the 4/2 resonance in the 6/2 base mode operation of the DED (The figure is used as a sketch for the similar situation in the 12/4 mode).

In Fig. 3 the unstable manifold crosses the wall first at about $\theta = 3.62$ turns around and reenters the system at about $\theta = 3.57$ (see also Fig. 4). This repeats at $\theta = 3$ and $\theta = 2.82$, respectively, until the manifold leaves the system totally at about $\theta = 2.52$. Note that the manifold is not a projection of a field line into the Poincaré section. The unstable manifold describes the unstable direction of the intersection points of field lines in the Poincaré section. So, not all field lines which follow the unstable manifold have to leave

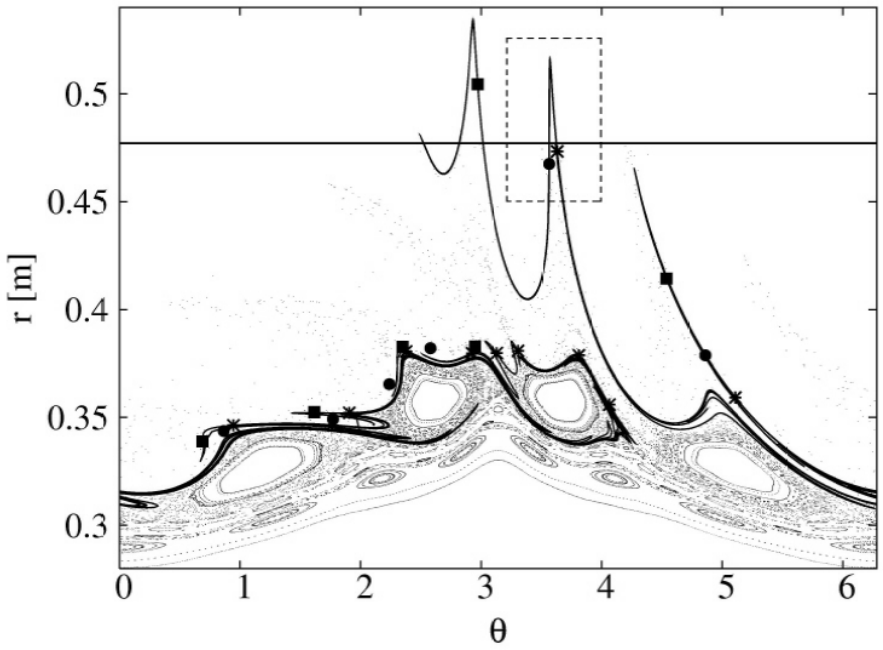

Figure 3: Poincaré section of the DED in 6/2 base mode operation with an unstable manifold (black line) of the 4/2 resonance at $q_a=3.16$. The manifold is continued beyond the first wall contact. The wall is drawn at $r=0.477$ m. The iteration of two different field lines is shown as dots and crosses, respectively.

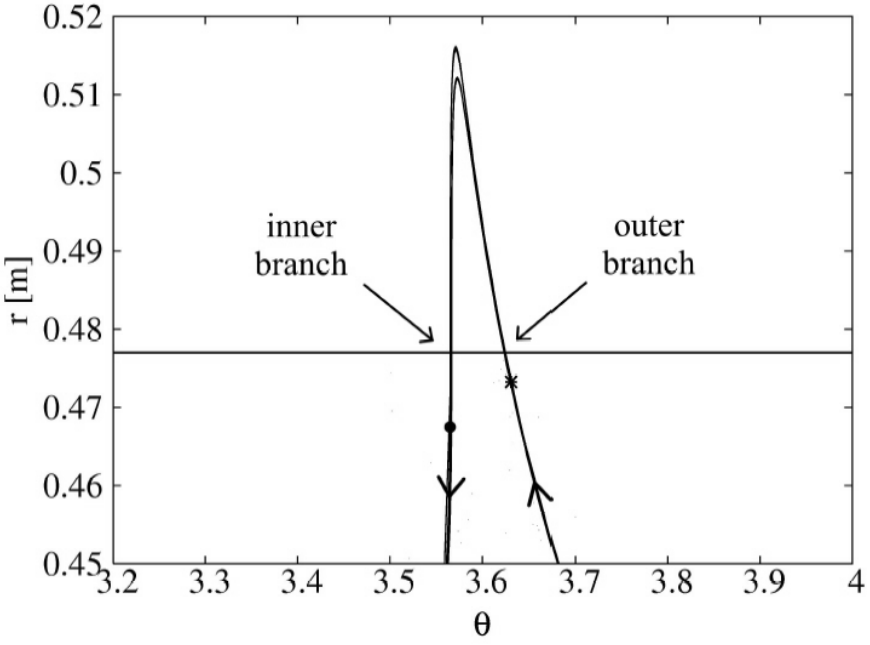

Figure 4: Magnification of the boxed area of Fig.3.

the system at the first wall contact of the manifold. Most do, but some skip the first loop and leave the system at the next outgoing wall intersection. This is also shown in Fig. 3 for three different field lines. One field line (the intersections are marked by dots) moves towards the wall and intersects the Poincaré section on the unstable manifold beyond the first external loop of the manifold. Note that the field line has not crossed the wall in between. The next intersection is already beyond the plotted area outside of the system. This field line has skipped the first external loop of the manifold. Another shown field line (the intersections are marked by crosses) intersects with the Poincaré section on the first outgoing part of the unstable manifold very close to the wall and the next time outside the system also already beyond the plotted area. This field line has left the system at the first wall contact of the manifold (at a slightly increased toroidal angle). The third shown field line (marked by squares) intersects the Poincaré section on the up going loop for the last time inside the system. The next intersection is already on the second external loop of the manifold. This field line has left the system either at the first or at the second outgoing wall contact of the manifold. All the discussed field lines have large connection lengthes. The important fact is that all particles following the field lines, strike the wall at the outgoing parts of the manifold.

According to these results, we can identify the inner and outer branches of the strike zones by the incoming and outgoing parts of the manifolds, respectively. The outer branches correspond to the experimentally observed areas of large heat fluxes. The inner branches, on the contrary, do not belong to an efficient particle transport from hot, inner areas towards the wall. Thus, it is understandable that they are not observed in the experiments, although the connection lengths are large. The topologies of the last intact island chains vary with q_a. Therefore, also the strike zones change with q_a, in accordance with experimental observations [49].

5 Summary

Summarizing, we have analyzed the development of typical heat flow patterns which appear due to ergodization of a plasma edge. For this purpose we concentrated on the TEXTOR-DED fusion experiment in Jülich. The magnetic field structure and the mapping technique was outlined, combined with the method to calculate stable and unstable manifolds. Measured heat flow patterns are related to large connection lengthes. But the stable and unstable manifolds of the hyperbolic points of the last intact island chain rule the characteristic heat deposition patterns. When connecting all relevant strike points of the stable and unstable manifolds, respectively, one exactly gets the heat flux pattern observed in the measurement.

6 Acknowledgments

The work is devoted to the great physicist Radu Balescu. We owe him many ideas and inspiration, continuous friendship and personal advice. We shall miss his scientific leadership and warm personality.

References

[1] R. Balescu, *Aspects of anomalous transport in plasmas*, (Institute of Physics Publishing, Bristol, 2005).

[2] R. Balescu, *Transport processes in plasmas: 2. Neoclassical transport theory*, (North-Holland, Amsterdam 1988).

[3] R.Balescu, *Statistical Dynamics: Matter out of Equilibrium*, (Imperial College Press, London, 1977).

[4] J. Guckenheimer and P. Holmes, *Nonlinear oscillations, dynamical systems, and bifurcations of vector fields*, (Springer, New York, 1983).

[5] F. Casse, M. Lemoine, and G. Pelletier, *Phys. Rev. D* **65**, 023002, (2001).

[6] A. Shalchi, J. W. Bieber, W. H. Matthaeus, and R. Schlickeiser, *Astrophys. J.* **642**, 230, (2006).

[7] W.M. Stacey, *Fusion Plasma Physics*, (Wiley-VCH, Weinheim, 2005).

[8] T.E. Evans, R. A. Moyer, K. H. Burrell, M. E. Fenstermacher, I. Joseph, A.W. Leonard, T. H. Osborne, G. D. Porter, M. J. Schaffer, P. Snyder, et al., *Nature Physics* **2**, 419 (2006).

[9] P. Ghendrih, A. Grossman, and H. Capes, *Plasma Phys. Control. Fusion* **38**, 1653 (1996).

[10] T. Evans, R. Moyer, P. Thomas, J. Watkins, T. Osborne, J. Boedo, E. Doyle, M. Fenstermacher, K. Finken, R. Groebner, et al., *Phys. Rev. Lett.* **92**, 235003 (2004).

[11] R. Balescu, M. Vlad, and F. Spineanu, *Phys. Rev. E* **58**, 951 (1998).

[12] R. Balescu, *Phys. Rev. E* **58**, 3781 (1998).

[13] S. S. Abdullaev, K. H. Finken, A. Kaleck, and K. H. Spatschek, *Phys. Plasmas* **5**, 196 (1998).

[14] S. S. Abdullaev, K. H. Finken, and K. H. Spatschek, *Phys. Plasmas* **6**, 153 (1999).

[15] K. H. Finken, S. S.Abdullaev, A. Kaleck, and G. H. Wolf, *Nuclear Fusion* **39**, 637 (1999).

[16] S. S.Abdullaev, *Nuclear Fusion* **44**, 12 (2004).

[17] K. H. Finken, S. S. Abdullaev, M. Jakubowski, M. Lehnen, A. Nicolai, and K. H. Spatschek, *The structure of magnetic field in the TEXTOR-DED*, vol. 45 of *Energy Technology* (Forschungszentrum Julich, Julich, Germany, 2005).

[18] S. S. Abdullaev, *Construction of Mappings for Hamiltonian Systems and Their Applications*, (Springer, Berlin, 2006).

[19] S. S. Abdullaev, *J. Phys. A: Math. Gen.* **35**, 2811 (2002).

[20] S. S.Abdullaev, *J. Phys. A: Math. Gen.* **32**, 2745 (1999).

[21] J. Wesson, *Tokamaks*, vol. 48, of *Oxford Engineering Science Series*, (Clarendon Press, Oxford, 2004), 3rd ed.

[22] A. Boozer, *Phys. Rev. Lett.* **49**, 786 (1982).

[23] R. B. White and Y. Wu, *Plasma Phys.Control. Fusion* **35**, 595 (1993).

[24] H. E. Mynick, *Phys. Fluids B* **5**, 1471, (1993).

[25] H. E. Mynick, *Phys. Fluids B* **5**, 2460, (1993).

[26] M. DeRover, N. J. LopesCardozo, and A. Montvai, *Phys. Plasmas* **3**, 4468 (1996).

[27] M. DeRover, N. J. LopesCardozo, and A. Montvai, *Phys. Plasmas* **3**, 4478 (1996).

[28] R. B. White, *Phys. Rev. E* **58**, 1774 (1998).

[29] M. DeRover, A. M. Schilham, A. Montvai, and N. J. LopesCardozo, *Phys. Plasmas* **6**, 2443 (1999).

[30] S. S. Abdullaev, A. Wingen, and K. H. Spatschek, *Phys. Plasmas* **13**, 042509 (2006).

[31] A. Wingen, S. Abdullaev, K. H. Finken, and K. H. Spatschek, *Nucl. Fusion* **46**, 941, (2006).

[32] M. Jakubowski, S. Abdullaev, K. Finken, and the TEXTOR team, *Nucl. Fusion* **44**, (2004).

[33] M. Jakubowski, S. Abdullaev, K. Finken, M. Lehnen, and the TEXTOR team, *J. Nucl.Mater.* **337-339**, 176, (2005).

[34] E.da Silva, I. Caldas, R. Viana, and M. Sanjuán, *Phys. Plasmas* **9**, 4917 (2002).

[35] S. S. Abdullaev, T. Eich, and K. H. Finken, *Phys. Plasmas* **8**, 2739 (2001).

[36] E. Nusse and J. A. Yorke, *Dynamics: Numerical explorations*, (Springer, New York, 1998).

[37] A. Wingen, K. H. Spatschek, and S. Abdullaev, *Contrib. Plasma Phys.* **45**, 500 (2005).

[38] T. E. Evans, R. K. Roeder, J. A. Carter, and B. I. Rapoport, *Contrib. Plasma Phys.* **44**, 235 (2004).

[39] T. E. Evans, R. K. Roeder, J. A. Carter, B. I. Rapoport, M. E. Fenstermacher, and C. J. Lasnier, *J. Phys.: Conf. Ser.* **7**, 174, (2005).

[40] A. H. Boozer, *Phys. Fluids* **26**, 1288 (1983).

[41] R. Balescu, *Transport processes in plasmas: 2. Neoclassical transport theory*, (North-Holland, Amsterdam, 1988).

[42] A. H. Boozer, in *Encyclopedia of Physical Science and Technology*, (Academic Press, New York, 1992), vol. 13.

[43] F. Nguyen, P. Ghendrih, and A. Samain, *Tech. Rep.DFRC/CAD Preprint EUR-CEA-FC-1539*, CEA, Cadarache (1995).

[44] S. S. Abdullaev, K. H. Finken, and K. H. Spatschek, *Phys. Plasmas* **6**, 153, (1999).

[45] S. S. Abdullaev, *Construction of Mappings for Hamiltonian Systems and Their Applications*, vol. 691, *of Lecture Notes in Physics*, (Springer-Verlag, Berlin Heidelberg, 2006).

[46] K. H. Finken and G. H. Wolf, *Fusion Eng. Design* **37**, 337 (1997).

[47] K. H. Finken, S. S. Abdullaev, A. Kaleck, and G. H. Wolf, *Nuclear Fusion* **39**, 637 (1999).

[48] M. W. Jakubowski, S. S. Abdullaev, K. H. Finken, M. Lehnen, and TEXTOR team, *Journal of Nuclear Materials* **337-339**, 176 (2005).

[49] M. W. Jakubowski, A. Wingen, S. S. Abdullaev, K. H. Finken, M. Lehnen, K. H. Spatschek, R. C. Wolf, and the TEXTOR team, *J. Nucl.Mater.* (2006), (submitted).

[50] S. S. Abdullaev, *J. Phys. A: Math. Gen.* **32**, 2745 (1999).

[51] S. S. Abdullaev, *J. Phys. A: Math. Gen.* **35**, 2811 (2002).

[52] J. H. Misguich, J.-D. Reuss, D. Constantinescu, G. Steinbrecher, M. Vlad, F. Spineanu, B. Weyssow, and R. Balescu, *Annales Physique* **28** 6, 87 (2003).

[53] G. Steinbrecher, J.-D. Reuss, and J. H. Misguich, *EUR-CEA-FC Report* p.1719 (2001).